Rotational excitation of HOCO$^+$ by helium at low temperature

K. Hammami[1], F. Lique[2], N. Jaïdane[1], Z. Ben Lakhdar[1], A. Spielfiedel[2], and N. Feautrier[2]

[1] Laboratoire de Physique Atomique, Moléculaire et Applications, Département de Physique, Faculté des Sciences,
Université de Tunis-Elmanar, Le Belvédère, 1060 Tunis, Tunisie
[2] LERMA and UMR 8112 of CNRS, Observatoire de Paris-Meudon, 92195 Meudon Cedex, France
e-mail: hammami283@yahoo.fr

ABSTRACT

Context. It has been shown that the HOCO$^+$ ion is present in interstellar space. As a large number of HOCO$^+$ lines can be observed in the millimeter and submillimeter wavelengths, this molecule is a useful tracer for both the temperature and the density structure of the clouds. Modeling of the spectra will require accurate radiative and collisional rates of species of astrophysical interest.
Aims. The paper focuses on the calculation of rotational excitation rate coefficients of HOCO$^+$ by He, useful for studies of low-temperature environments.
Methods. Cross sections are calculated using the quantum Coupled States approach for a total energy range 0–200 cm^{-1}. These calculations are based on a new ab initio CEPA (coupled electron pair approach) potential energy surface. It was assumed that the HOCO$^+$ ion was fixed at its theoretical equilibrium geometry.
Results. Thermally averaged rate coefficients were calculated from the cross sections, at kinetic temperatures up to 30 K.

Key words. ISM: molecules – molecular processes – molecular data

1. Introduction

It has been shown that HOCO$^+$ is present in interstellar space (Thaddeus et al. 1981; Cummins et al. 1986; Minh et al. 1988) by observing the rotational lines ($1_{01} \rightarrow 0_{00}$, $4_{04} \rightarrow 3_{03}$, $4_{14} \rightarrow 3_{13}$, $4_{13} \rightarrow 3_{12}$, $5_{05} \rightarrow 4_{04}$, $6_{06} \rightarrow 5_{05}$...) emitted by a combination of radiative and collisional processes. The wide variety of HOCO$^+$ lines accessible in the millimeter and submillimeter wavelengths are useful to trace both the temperature and the density structure of the clouds. In addition, due to their large dipole moment, HOCO$^+$, like many other ions (CH$^+$, HCO$^+$, N$_2$H$^+$), allows to trace regions of different densities. These species play an important role in the chemistry of interstellar and circumstellar environments. In order to interpret the observations of HOCO$^+$, spectroscopic data as well as collisional rate coefficients are required, the most important perturbers being H$_2$ and He. To our knowledge, no collisional data are presently available for HOCO$^+$. We present in this paper cross sections and rate coefficients for rotational excitation by He.

HOCO$^+$ is an asymmetric top molecule. The quantum mechanical close coupling (CC) method gives the most accurate results for low-energy scattering. However, due to the large number of low lying states in HOCO$^+$, CC calculations are not currently feasible and we adopt here the coupled states (CS) theory, first introduced by McGuire & Kouri (1974) and Pack (1974) and extended by Garrison & Lester (1977) to the case of atom-asymmetric top scattering. For the present study, we used the HOCO$^+$-He interaction potential calculated by Hammami et al. (2004) with the ab initio Coupled Electron Pair Approximation (CEPA) reported by Meyer (1971). This potential has been used to compute inelastic cross sections for the 25 first rotational levels and total energies up to 200 cm^{-1}. Rate coefficients were thus obtained by averaging these cross sections over a Boltzman distribution of velocities for temperatures ranging from 5 to 30 K.

2. Potential energy surface

The interaction energy of the HOCO$^+$-He system was calculated at the CEPA level (Meyer 1971) using the Correlation Consistent Polarized Triple Zeta basis set of Dunning (1989) augmented with the diffuse functions (s, p, d symmetries for H, s, p, d, f symmetries for C and O) of Kendall et al. (1992). The distances and angles of the HOCO$^+$ molecule were assumed fixed at their theoretical equilibrium geometry (see Table 1 and Fig. 1). The equilibrium coordinates obtained from a CEPA calculation compare well with the experimental data (Hammami et al. 2004). Details of the calculations and plots of the interaction energy are given in Hammami et al. (2004).

The interaction energy may be expressed in the following functional form:

$$V(R', \Theta', \Phi') =$$
$$\sum_{\lambda=0}^{\infty} \sum_{\eta=0}^{\lambda} v_{\lambda\eta}(R') \frac{Y_{\lambda\eta}(\Theta', \Phi') + (-1)^\eta Y_{\lambda-\eta}(\Theta', \Phi')}{1 + \delta_{\eta 0}} \quad (1)$$

where $\delta_{\eta 0}$ is a delta function. R', Θ', Φ' are the spherical polar coordinates of the helium atom with respect to the coordinate system fixed to the molecule. $Y_{\lambda\eta}(\Theta', \Phi')$ denotes a normalized spherical harmonic function.

To obtain a global representation of the interaction energy in an analytic form, the R'-dependence of the $v_{\lambda\eta}(R')$ functions was extrapolated at the short distances ($R' \leq 4$ bohr) by an exponential function $A_{\lambda\eta} \exp(-B_{\lambda\eta}R')$. At large distances ($R' \geq 10$ bohr), the $v_{\lambda\eta}(R')$ functions were extrapolated by an inverse power expansion:

$$v_{\lambda\eta}(R') = \sum_n C_{\lambda\eta}^n R'^{-n}. \quad (2)$$

Table 1. Calculated structure of HOCO$^+$, lengths are in angstroms and angles in degrees.

H-O	O–C	C–O	∠ HOC	∠ OCO
0.984	1.229	1.124	117.6	174.3
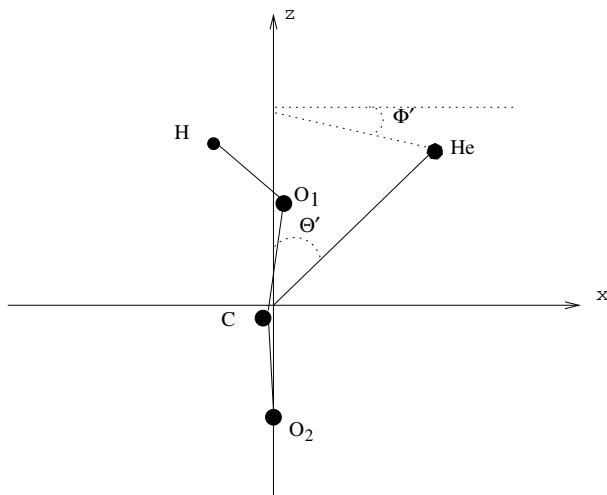
Fig. 1. Coordinate system and geometry of HOCO$^+$.

We have included in the dynamics calculations all the λ and η terms up to $\lambda, \eta = 5$.

3. Collision treatment

3.1. Hamiltonian and HOCO$^+$ rotational eigenstates and eigenenergies

We consider here the collision of the asymetric top molecule HOCO$^+$ with He atoms. The Hamiltonian of this system in space-fixed coordinates with the origin at the centre of mass of the rigid rotor is expressed as (Arthurs & Dalgarno 1960):

$$H = H_{\text{rot}}(\widehat{r}) + V(\widehat{r}, \boldsymbol{R}) + T(\boldsymbol{R}) \tag{3}$$

where H_{rot} represents the rotational Hamiltonian of HOCO$^+$, $T(\boldsymbol{R})$ is the kinetic energy operator and $V(\widehat{r}, \boldsymbol{R})$ is the electronic interaction energy of the HOCO$^+$−He system. $\widehat{r}$ are the Euler angles which describe the rotation of the space-fixed reference frame into the body-fixed reference frame. $\boldsymbol{R}$ is the vector from the asymmetric top center of mass to the atom in space-fixed coordinates.

HOCO$^+$ is an asymmetric rotor described by the following Hamiltonian in the fixed-molecule coordinate system:

$$H_{\text{rot}} = \frac{J_x^2}{2I_x} + \frac{J_y^2}{2I_y} + \frac{J_z^2}{2I_z} \tag{4}$$

where I_α ($\alpha = x, y, z$) are the principal moments of inertia and $\widehat{J_\alpha}$ are the angular momentum operators of HOCO$^+$ about the principal axis (oα). o is the centre of mass of the HOCO$^+$ ion. I_x, I_y and I_z are related to the rotational constants according to $A = 1/2I_x$, $B = 1/2I_y$ and $C = 1/2I_z$.

The asymmetric top wave functions $|j\tau m\rangle$ are therefore expanded over the basis of eigenfunctions of the symmetric rigid rotor $|jkm\rangle$ (Townes & Schawlow 1955):

$$|j\tau m\rangle = \sum_k a_{\tau,k}^j |jkm\rangle \tag{5}$$

Table 2. Rotational energy (in cm^{-1}) calculated for the lowest levels from the theoretical (^{a}) and the experimental (^{b} Amano & Tanaka 1985) constants.

j	τ	$k_{\text{a}}, k_{\text{c}}$	$E_{j,\tau}{}^a$	$E_{j,\tau}{}^b$
0	0	0, 0	0.0000	0.0000
1	−1	0, 1	0.7111	0.7133
2	−2	0, 2	2.1333	2.1399
3	−3	0, 3	4.2666	4.2798
4	−4	0, 4	7.1110	7.1330
5	−5	0, 5	10.6665	10.6995
6	−6	0, 6	14.9330	14.9792
7	−7	0, 7	19.9107	19.9723
1	0	1, 1	25.3564	26.7007
1	1	1, 0	25.3615	26.7007
8	−8	0, 8	25.5994	25.6786
2	−1	1, 2	26.7736	28.1218
2	0	1, 1	26.7887	28.1383
3	−2	1, 3	28.8993	30.2535
3	−1	1, 2	28.9295	30.2864
4	−3	1, 4	31.7337	33.0958
4	−2	1, 3	31.7840	33.1505
9	−9	0, 9	31.9992	32.0982
5	−4	1, 5	35.2766	36.6486
5	−3	1, 4	35.3521	36.7307
10	−10	0, 10	39.1101	39.2310
6	−5	1, 6	39.5281	40.9120
6	−4	1, 5	39.6338	41.0269
7	−6	1, 7	44.4881	45.8859
7	−5	1, 6	44.6291	46.0391
11	−11	0, 11	46.9320	47.0771
8	−7	1, 8	50.1568	51.5704
8	−6	1, 7	50.3380	51.76735
12	−12	0, 12	55.4649	55.6365
9	−8	1,9	56.5340	57.9654
9	−7	1,8	56.7605	58.8116
10	−9	1,10	63.6198	65.0710
10	−8	1,9	63.8966	65.3719

where j, k, m and τ denote respectively the total angular momentum of the molecule, its projection along the molecule z-axis, its projection along the space-fixed Z-axis, and τ is an index introduced to identify the asymmetric wave-functions. The $|jkm\rangle$ are:

$$|jkm\rangle = \sqrt{\frac{2j+1}{8\pi^2}} D_{km}^j(\alpha, \beta, \gamma) \tag{6}$$

D_{km}^j is a rotation matrix defined according to the convention of Edmonds (1960). The coefficients $a_{\tau,k}^j$ may be obtained by diagonalizing the asymmetric rigid rotor Hamiltonian as discussed by Green (1976) which gives the required matrix elements.

The rotational levels of HOCO$^+$ are also conventionally labeled $j_{k_p k_o} \equiv j_{k_a k_c}$, where $k_p(k_o)$ and $k_a(k_c)$ are the k quantum numbers in the prolate and oblate limits, k_a and k_c being related to τ through $\tau = k_a - k_c$. The $j_{k_a k_c}$ notation will be adopted hereafter. None of the k are good quantum numbers, but the asymmetric top Hamiltonian conserves the symmetry (even or odd) of each k (Hutson 1990).

The rotational energy levels $E_{j_{k_a k_c}}$ (i.e. $E_{j\tau}$) of HOCO$^+$ were computed from the ab initio calculated rotational constants ($A = 0.358$ cm^{-1}, $B = 0.353$ cm^{-1} and $C = 25.003$ cm^{-1}, Hammami et al. 2004) using the ASROT subroutine of the MOLSCAT computer program (Hutson & Green 1995). The results are presented in Table 2 for the lowest levels.
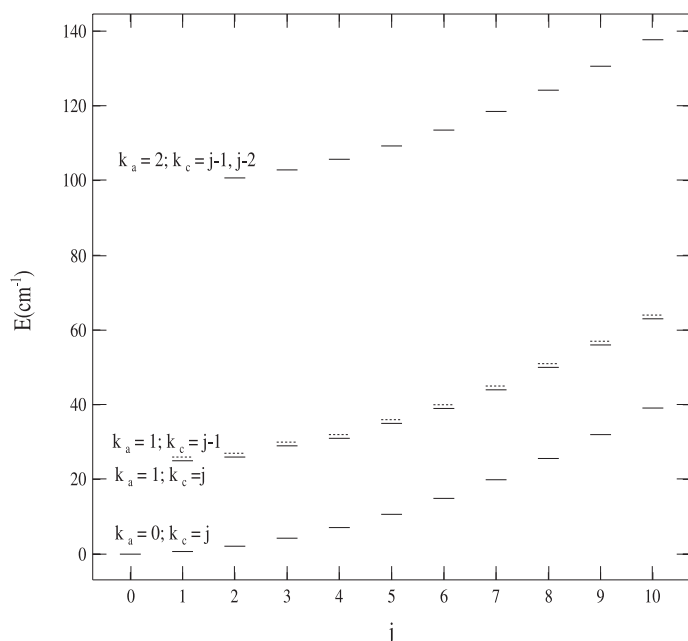
Fig. 2. Rotational HOCO$^+$ levels for j up to 10.

The comparison with the energies deduced from the experimental values shows that the energy level structure is reproduced satisfactorily exept for the 8_{08} level (inverted with the 1_{11} and 1_{10} levels) and the 9_{09} level (inverted with the 4_{14} and 4_{13} levels). In Fig. 2 we plot the first energy levels of HOCO$^+$; the rotational structure is complex and the energy spacing between the levels is small. Comparison of the calculated frequencies with the observed ones (Thaddeus 1981) and with the values deduced from experiments (Amano & Tanaka 1985; Bogey et al. 1986) shows a very good agreement (Table 3).

3.2. Dynamics of HOCO$^+$-He collisions

The close coupling (CC) quantum theory of Arthurs & Dalgarno (1960), first introduced for atom-diatom collisions at low energies, was extended for atom-asymmetric top collisions by Garrison et al. (1976) and then by Garrison & Lester (1977) in the coupled states (CS) approximation. This approximation has been used for complex collisional systems, such as He in collision with H$_2$CO (Green et al. 1978), CH$_3$CN (Green 1985), CH$_3$OH (Pottage et al. 2001), H$_2$ in collision with H$_2$O (Phillips et al. 1995). The present calculations were performed with the MOLSCAT code of Hutson & Green (1995) in the atom-asymmetric top CS approximation and with the log-derivative method of Manolopoulos (1986).

A series of calculations was carried out in order to test the convergence of the HOCO$^+$ cross sections with respect to increasing the rotational basis set. Tests were done until $j_{max} = 14$. Convergence as a function of the basis set size was obtained from $j_{max} = 10$ within 20–30% of error with respect to $j_{max} = 14$. This poor basis set convergence is related to the deep potential well ($\simeq 400$ cm^{-1}) compared to the energy splitting and to the strong anisotropy of the interaction energy (Green 1976). A strong resonance structure is thus expected in the cross sections. As the size of the coupled equations and the necessary computer time to solve them increase very rapidly with the size of the basis set, we have adopted the computationally feasible $j_{max} = 12$ basis set. We thus estimate being able to obtain state-to-state cross sections
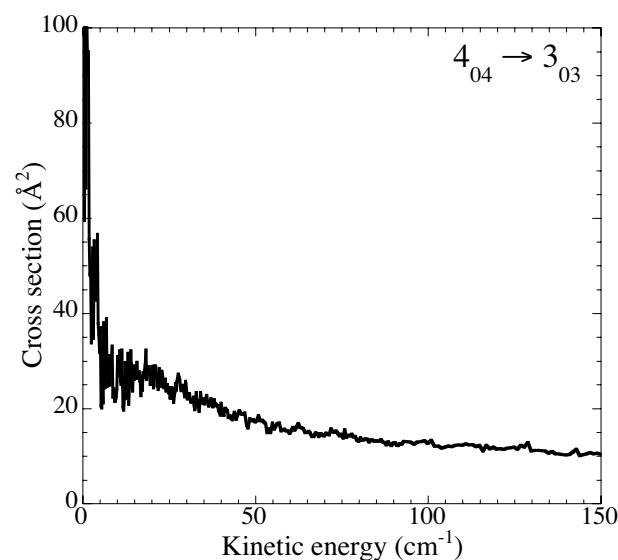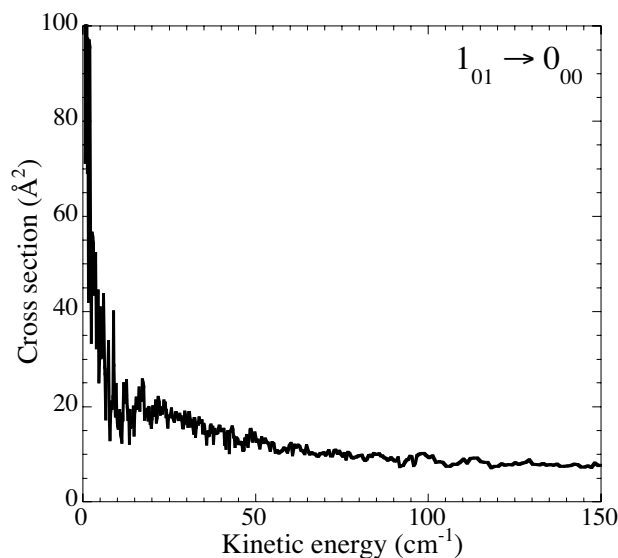

Fig. 3. Typical collisional de-excitation cross sections of HOCO$^+$ by He.

and rate coefficients accurate within 30–40%. The propagation parameters used in the calculations are displayed in Table 4.

4. Results and discussion

Figure 3 presents the typical energy dependence of the cross sections. All the cross sections exhibit strong resonances; a small energy step is required to correctly represent the resonances.

The cross sections were integrated over the Maxwell-Boltzmann distribution of kinetic energies in order to obtain the collision rate coefficients.

$$q_{jk_ak_c \to j'k_a'k_c'}(T) =$$
$$\left(\frac{8\beta^3}{\pi\mu}\right)^{1/2} \int_0^\infty E_c \sigma_{jk_ak_c \to j'k_a'k_c'}(E) e^{-\beta E_c} dE_c \qquad (7)$$

where T is the kinetic temperature, μ is the reduced mass of the HOCO$^+$-He collision partners, $\beta = \frac{1}{k_BT}$, k_B is the Boltzmann constant and $E_c = E - E_{j_{k_ak_c}}$ is the relative kinetic energy.

Table 3. Comparison between transition frequencies (in GHz) calculated in this work ν_{cal}, calculated from experimental work (ν_{exp} [b] Amano & Tanaka 1985; [c] Bogey et al. 1986) and observed values ([a] Thaddeus et al. 1981, ν_{obs}).

Transitions	ν_{cal}	ν_{exp} [b]	ν_{exp} [c]	ν_{obs} [a]
$1_{01} \to 0_{00}$	21.318067	21.38312		21.38280[a]
$2_{02} \to 1_{01}$	42.636134	42.76613		
$3_{03} \to 2_{02}$	63.953001	64.14893		
$4_{04} \to 3_{03}$	85.271968	85.53139		85.53068[a]
$5_{05} \to 4_{04}$	106.589735	106.91341		106.91336[a]
$6_{06} \to 5_{05}$	127.907502	128.29487		128.29489[a]
$2_{11} \to 1_{10}$	42.786928	42.92662		
$2_{12} \to 1_{11}$	42.485339	42.59835		
$3_{12} \to 2_{11}$	64.180242	64.38970		
$3_{13} \to 2_{12}$	63.727859	63.89729		
$4_{13} \to 3_{12}$	85.573856	85.85252	85.85281	
$4_{14} \to 3_{13}$	84.970079	85.19596	85.19572	
$5_{14} \to 4_{13}$	106.967470	107.31497		
$5_{15} \to 4_{14}$	106.212899	106.49427		
$6_{15} \to 5_{14}$	128.360485	128.77697		
$6_{16} \to 5_{15}$	127.455419	127.79211		
$3_{21} \to 2_{20}$	63.954201	64.12707		
$3_{22} \to 2_{21}$	63.954201	64.12697		
$4_{22} \to 3_{21}$	85.272268			
$4_{23} \to 3_{22}$	85.271968			
$5_{23} \to 4_{22}$	106.590634			
$5_{24} \to 4_{23}$	106.590035			
$6_{24} \to 5_{23}$	127.909001			
$6_{25} \to 5_{24}$	127.908401			

Table 4. MOLSCAT parameters used in present calculations.

INTFLG = 6	STEPS = 10	OTOL = 0.005	JMAX = 12
A = 0.358 cm^{-1}	B = 0.353 cm^{-1}	C = 25.003 cm^{-1}	EMAX = 300 cm^{-1}
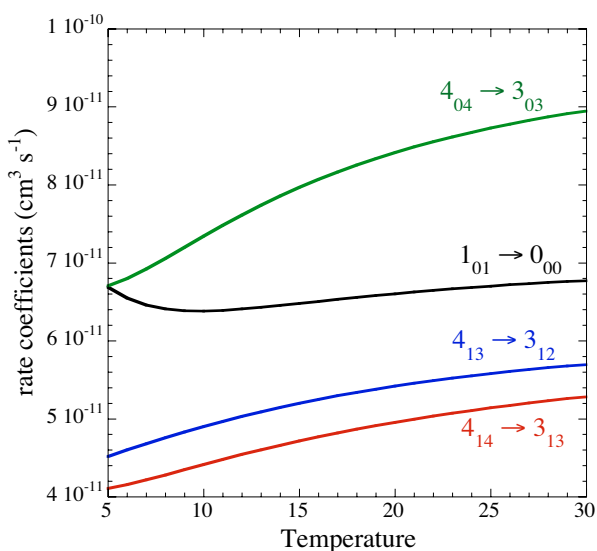
Fig. 4. Downward rate coefficients of HOCO$^+$ in collision with He, as a function of the temperature.
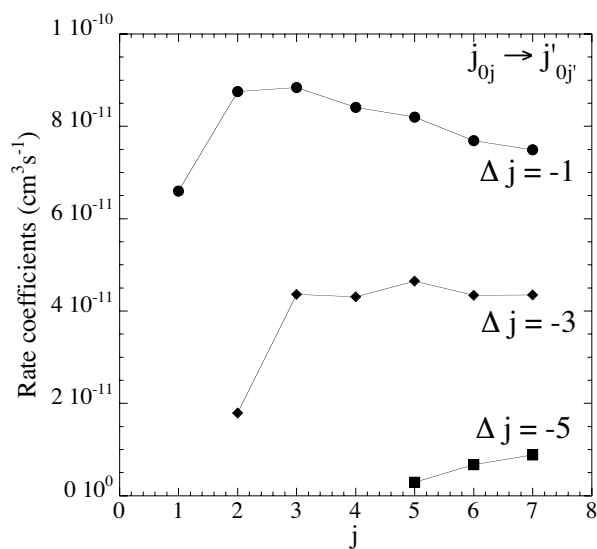
Fig. 5. Variation with the initial j value of the downward rate coefficients for different Δj values: $\Delta k_a = 0$, $\Delta k_c = \Delta j$. $T = 20$ K.

Calculations were performed with an energy step of 0.2 cm^{-1} from 1 to 50 cm^{-1}, 0.5 cm^{-1} from 50 to 100 cm^{-1}, and 1.0 cm^{-1} from 100 to 200 cm^{-1}. The rate coefficients for the 25 first levels were calculated from 5 K to 30 K with a temperature step of 5 K. The results for the 10 first levels are displayed in Table 5 at 10 K, 20 K and 30 K. The complete set of rate coefficients will be made available in the BASECOL database (`http://www.obspm.fr/basecol`). The typical variation of the downward rate coefficients is shown in Fig. 4.

In order to establish collisional propensity rules, we present the de-excitation rate coefficients for inelastic transitions at a kinetic temperature of 20 K in the form of plots as a function of the initial j value. In Fig. 5, we present the rate coefficients for $\Delta k_a = 0, \Delta k_c = \Delta j$ for different $\Delta j = j' - j$ values.

Table 5. Downward rate coefficients between initial (i) and final (f) levels of HOCO$^+$ as a function of the kinetic temperature (units are cm^3 s^{-1}).

i	f	10 K	20 K	30 K	i	f	10 K	20 K	30 K
1_{01}	0_{00}	6.38e-11	6.60e-11	6.77e-11	7_{07}	2_{02}	1.17e-11	8.87e-12	7.58e-12
2_{02}	0_{00}	1.83e-11	1.79e-11	1.72e-11	7_{07}	3_{03}	2.26e-11	1.79e-11	1.56e-11
2_{02}	1_{01}	8.42e-11	8.75e-11	8.95e-11	7_{07}	4_{04}	2.25e-11	1.88e-11	1.71e-11
3_{03}	0_{00}	1.05e-11	8.97e-12	8.03e-12	7_{07}	5_{05}	4.79e-11	4.35e-11	4.06e-11
3_{03}	1_{01}	4.49e-11	4.36e-11	4.10e-11	7_{07}	6_{06}	7.13e-11	7.49e-11	7.83e-11
3_{03}	2_{02}	7.81e-11	8.84e-11	9.29e-11	1_{11}	0_{00}	2.51e-11	3.01e-11	3.34e-11
4_{04}	0_{00}	9.45e-12	9.25e-12	8.66e-12	1_{11}	1_{01}	2.53e-11	2.03e-11	1.83e-11
4_{04}	1_{01}	1.87e-11	1.70e-11	1.55e-11	1_{11}	2_{02}	4.26e-11	4.05e-11	3.96e-11
4_{04}	2_{02}	4.51e-11	4.31e-11	4.07e-11	1_{11}	3_{03}	2.77e-11	2.18e-11	2.00e-11
4_{04}	3_{03}	7.34e-11	8.41e-11	8.95e-11	1_{11}	4_{04}	3.42e-11	2.79e-11	2.47e-11
5_{05}	0_{00}	3.04e-12	2.91e-12	2.77e-12	1_{11}	5_{05}	2.52e-11	2.04e-11	1.82e-11
5_{05}	1_{01}	1.56e-11	1.42e-11	1.32e-11	1_{11}	6_{06}	3.16e-11	2.49e-11	2.16e-11
5_{05}	2_{02}	2.11e-11	1.86e-11	1.70e-11	1_{11}	7_{07}	2.16e-11	1.87e-11	1.70e-11
5_{05}	3_{03}	5.00e-11	4.65e-11	4.33e-11	1_{10}	0_{00}	0.00[a]	0.00[a]	0.00[a]
5_{05}	4_{04}	7.29e-11	8.20e-11	8.68e-11	1_{10}	1_{01}	3.76e-11	4.59e-11	5.13e-11
6_{06}	0_{00}	2.31e-12	2.03e-12	1.90e-12	1_{10}	2_{02}	2.33e-11	1.96e-11	1.91e-11
6_{06}	1_{01}	8.50e-12	6.76e-12	5.95e-12	1_{10}	3_{03}	3.33e-11	2.88e-11	2.62e-11
6_{06}	2_{02}	1.79e-11	1.56e-11	1.44e-11	1_{10}	4_{04}	1.61e-11	1.44e-11	1.38e-11
6_{06}	3_{03}	2.40e-11	2.07e-11	1.88e-11	1_{10}	5_{05}	2.51e-11	2.03e-11	1.74e-11
6_{06}	4_{04}	4.66e-11	4.34e-11	4.08e-11	1_{10}	6_{06}	1.92e-11	1.46e-11	1.29e-11
6_{06}	5_{05}	6.90e-11	7.69e-11	8.18e-11	1_{10}	7_{07}	1.54e-11	1.29e-11	1.19e-11
7_{07}	0_{00}	2.11e-12	1.69e-12	1.48e-12	1_{10}	1_{11}	6.19e-11	6.66e-11	6.75e-11
7_{07}	1_{01}	5.63e-12	4.66e-12	4.25e-12					

[a] These rate coefficients are identically zero in the coupled states approximation.
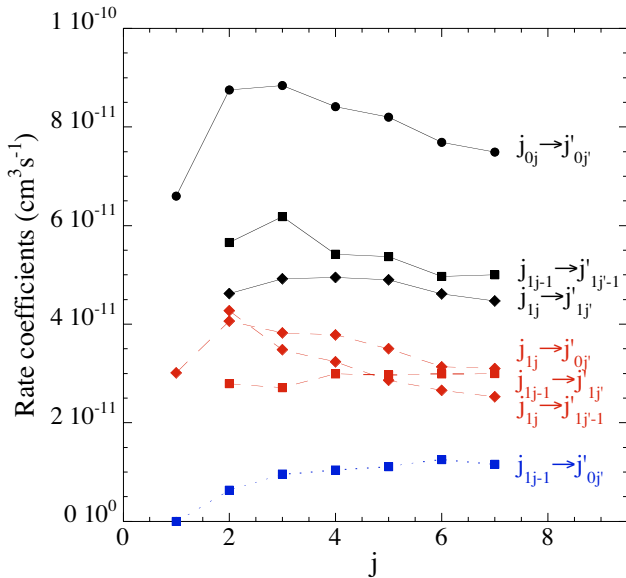

Fig. 6. Variation with the initial j value of the downward rate coefficients for $\Delta j = -1$ and different types of transitions. $T = 20$ K. full line: $\Delta k_a = 0$, $\Delta k_c = \Delta j$; broken line: $\Delta k_a \neq 0$ or $\Delta k_c \neq \Delta j$; dotted line: $\Delta k_a \neq 0$ and $\Delta k_c \neq \Delta j$.

Fig. 7. Variation with the initial j value of the downward rate coefficients for $\Delta j = 0$. $T = 20$ K.

The results show that the rate coefficients decrease with increasing Δj. This propensity is the usual trend and was found for other systems like CH$_3$OH-He (Pottage et al. 2001).

In Figs. 6 and 7 we present the rate coefficients for $\Delta j = -1$ and $\Delta j = 0$. For $\Delta j = -1$ (and for all $|\Delta j| > 1$ not shown here), we find a clear propensity for transitions with $\Delta k_a = 0, \Delta k_c = \Delta j$; the rate coefficients for transitions involving $\Delta k_a \neq 0$ or $\Delta k_c \neq \Delta j$ are smaller and they are very small for transitions with $\Delta k_a \neq 0$ and $\Delta k_c \neq \Delta j$. Considering transitions with $\Delta j = 0$, it appears that the $j_{1j-1} \rightarrow j_{0j}$ rate coefficient is of the same
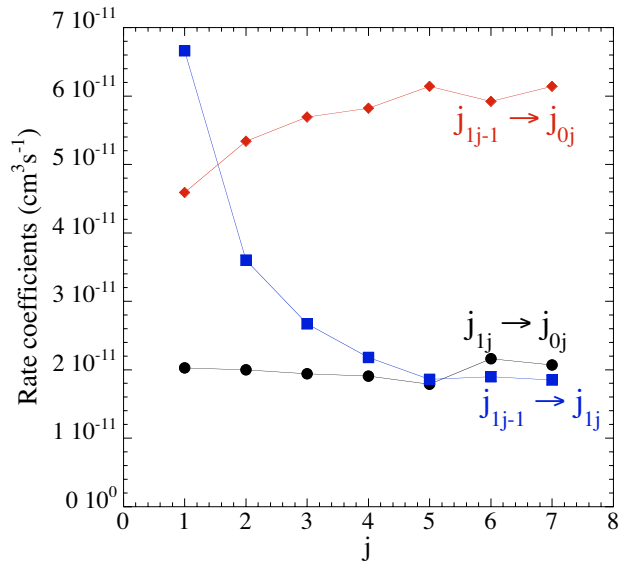
order of magnitude as the rate coefficients for $\Delta j = -1$ and $\Delta k_a = 0, \Delta k_c = \Delta j$; the rate coefficients for the two other transitions are small for large j.

In conclusion, we estimate from this study that (in spite of convergence difficulties) the method used in this work gives an estimate for rates of the HOCO$^+$-He system that are of acceptable accuracy for many applications including preliminary astronomical modeling. In particular, the propensity rules give a correct description of the relative importance of the different state-to-state rate coefficients.

References

Amano, T., & Tanaka, K. 1985, J. Chem. Phys., 83, 3721

Arthurs, A. M., & Dalgarno, A. 1960, Proc. Roy. Soc. London, Ser. A, 256, 540

Bogey, M., Demuynck, C., & Destombes, J. L. 1986, J. Chem. Phys., 84, 10

Cummins, S. E., Linke, R. A., & Thaddeus, P. 1986, ApJS, 60, 819

Dunning, T. H. Jr. 1989, J. Chem. Phys., 90, 1007

Edmonds, A. P. 1960, Angular Momentum in Quantum Mechanics (Princeton: Princeton University)

Garrison, J., Lester, W. A., & Miller, W. H. 1976, J. Chem. Phys., 65, 2193

Garrison, B. J., & Lester, W. A. 1977, J. Chem. Phys., 66, 631

Green, S. 1976, J. Chem. Phys., 64, 3463

Green, S., Garrison, B. J., Lester, W. A., & Miller, W. H. 1978, ApJS, 37, 321

Green, S. 1985, J. Chem. Phys., 89, 5289

Hammami, K., Jaidane, N., Ben Lakhdar, Z., Spielfiedel, A., & Feautrier, N. 2004, J. Chem. Phys., 121, 1325

Hutson, J. 1990, J. Chem. Phys., 92, 157

Hutson, J. M., & Green, S. 1995, MOLSCAT computer code, version 14, Distributed by Collaborative Computational Project 6 (Warington, UK: Daresbury Laboratory)

Kendall, R. A., Dunning, T. H. Jr., & Harrison, R. J. 1992, J. Chem. Phys., 96, 6769

Manolopoulos, D. E. 1986, J. Chem. Phys., 85, 6425

McGuire, P., & Kouri, D. J. 1974, J. Chem. Phys., 60, 7488

Meyer, W. 1971, Int. J. Quant. Chem., Symp., 5, 341

Minh, Y. C., Irvine, W. M., & Ziurys, L. M. 1988, ApJ, 334, 175

Pack, R. T. 1974, J. Chem. Phys., 60, 633

Pottage, J. T., Flower, D. R., & Davis, S. L. 2001, J. Phys. B., 34, 3313

Phillips, T. R., Maluendes, S., & Green, S. 1995, J. Chem. Phys., 102, 6024

Thaddeus, P., Guélin, M., & Linke, R. A. 1981, ApJ, 246, L41

Townes, C. H., & Schawlow, A. L. 1955, Microwave Spectroscopy (New York: McGraw Hill)